Met. Mater. Int., Vol. 19, No. 5 (2013), pp. 901~906
doi: 10.1007/s12540-013-5001-7

Kinetic Study of Non-Isothermal Crystallization in $Al_{80}Fe_{10}Ti_5Ni_5$ Metallic Glass

M. Tavoosi[1,2,3], F. Karimzadeh[2], M. H. Enayati[2], S. Lee[3], and H. S. Kim[3,*]

[1]Malek-Ashtar University of Technology (MUT), Department of Material Engineering, Shahin-shahr, Isfahan, Iran
[2]Isfahan University of Technology (IUT), Nanotechnology and Advanced Material Institute, Department of Material Engineering, Isfahan 84156-83111, Iran
[3]Pohang University of Science and Technology (POSTECH), Department of Materials Science and Engineering, Pohang 790-784, Korea

(received date: 28 April 2012 / accepted date: 28 December 2012)

This study investigated the crystallization behavior of a kinetically metastable $Al_{80}Fe_{10}Ti_5Ni_5$ amorphous phase. The $Al_{80}Fe_{10}Ti_5Ni_5$ amorphous phase was synthesized via the mechanical alloying of elemental powders of Al, Fe, Ti, and Ni. The microstructures and crystallization kinetics of the as-milled and annealed powders were characterized using X-ray diffraction, transition electron microscopy, and non-isothermal differential thermal analysis techniques. The results demonstrated that an $Al_{80}Fe_{10}Ti_5Ni_5$ amorphous phase was obtained after 40 h of ball milling. The produced amorphous phase exhibited one-stage crystallization on heating, i.e., the amorphous phase transforms into nanocrystalline $Al_{13}(Fe,Ni)_4$ (40 nm) and Al_3Ti (10 nm) intermetallic phases. The activation energy for the crystallization of the alloy evaluated from the Kissinger equation was approximately 538±5 kJ/mol using the peak temperature of the exothermic reaction. The Avrami exponent or reaction order *n* indicates that the nucleation rate decreases with time and the crystallization is governed by a three-dimensional diffusion-controlled growth. These results provide new opportunities for structure control through innovative alloy design and processing techniques.

Key words: amorphous materials, nanostructured materials, mechanical alloying, crystallization, phase transformation

1. INTRODUCTION

Structural materials with high-specic strength are consistently of considerable interest to the transportation and aviation industries. Thus, the development of Al-based alloys is eagerly awaited in these industries due to its perceived benefits. The main advantages of Al-based alloys are low density and good corrosion resistance [1-6]. A new class of Al-based alloys, which have received much attention recently, is amorphous as well as nanocrystalline alloys [7-17]. Amorphous alloys are sufficiently adaptable and they have an unusual combination of properties such as high strength, good ductility, high fracture toughness, and good corrosion resistance.

Among the Al alloys, Al-Fe systems are of technological interest because they have advantageous properties including high specific strength, high specific stiffness, good strength at intermediate temperatures, and excellent corrosion resistance at elevated temperatures in oxidizing and carburizing atmospheres. In fact, the alloys in the Al-rich side of the Al-Fe alloying system have low glass forming ability and the stability of the glass phase in these alloying systems are quite low. It is clear that, by addition of one or more alloying elements to these systems, the glass forming ability and the thermal stability of amorphous phase can be improved. For instance, in our previous study, we reported that by adding Ti, Ni, and V elements to $Al_{80}Fe_{10}M_{10}$ (M=Ti, Ni, and V) alloys, the glass forming ability and thermal stability of their amorphous phases increased [14]. The results showed that the effect of these alloying elements on Al-Fe alloys is not the same and the thermal stability of the produced amorphous phase decreases in the order of $Al_{80}Fe_{10}Ti_{10}$>$Al_{80}Fe_{10}Ni_{10}$ >$Al_{80}Fe_{10}V_{10}$ [14].

It has been shown that this type of alloy can be prepared using either melt spinning or mechanical alloying (MA) techniques. MA is a solid-state powder processing technique involving repeated deformation, welding, and fracturing of the powder particles [18]. This technique has been widely used to synthesize a variety of materials, such as amorphous, nanocrystalline, and composite materials [6,15,13,19-25].

Metallic glasses are kinetically metastable materials. It is generally known that the high strength and good bending

*Corresponding author: hskim@postech.ac.kr

ductility of amorphous alloys are lost via annealing-induced crystallization. However, in the past decade, a substantial increase in strength from the annealing-induced crystallization has been reported in a number of multiphase nanocrystalline alloys. The bulk amorphous alloys with nanocrystalline dispersoids (nanocrystals dispersed in amorphous matrix) have a much improved strength compared with that of fully amorphous alloys [8]. Hence, the kinetics of the crystallization of an amorphous system is a key subject for study since it provides new opportunities for structure control through innovative alloy design and processing techniques.

In our previous study [14], we added the Ti and Ni elements to $Al_{80}Fe_{10}M_{10}$ (M=Ti, Ni) alloys and found that these elements can increase the glass forming ability and thermal stability of the amorphous phase due to high atomic interaction between these elements with Al (the atomic interaction between Al, Ti, and Ni is high). Thus, the aim of this work is study the effect of the simultaneous presence of Ti and Ni on glass the forming ability (during mechanical alloying) and thermal stability of the amorphous phase in the $Al_{80}Fe_{10}Ti_5Ni_5$ alloy. We studied the structural changes during MA and the heating and thermal behavior of the milling products. Moreover, we also investigated the activation energies of the crystallization in addition to other kinetic parameters (such as the Avrami exponent n) which describe the crystallization mechanism of the amorphous phase.

2. EXPERIMENTAL PROCEDURES

The powders of Al (99%), Fe (99.9%), Ti (99%), and Ni (99.99%) were used as raw materials. The elemental powders with a composition of $Al_{80}Fe_{10}Ti_5Ni_5$ were mechanically alloyed in a planetary ball mill in an argon atmosphere. The MA was performed in a steel container at room temperature. A rotation speed of 250 rpm and ball to powder ratio of 10:1 was employed. One mass% stearic acid powder supplied by Merck was used as the process control agent (PCA).

X-ray diffraction (XRD) was used to follow the structural changes of the powders during the milling and subsequence annealing. A Philips diffractometer (40 kV) with Cu Kα radiation (θ=0.15406 nm) was used for the XRD measurements. The XRD patterns were recorded in a 2θ range of 20-100° (step size: 0.03°; time per step: 1 s). The crystalline sizes of the phases formed during crystallization of the amorphous phase were estimated from the broadening of the XRD peaks using the Williamson-Hall formula [26]. The microstructure of the produced amorphous powder was investigated using a high resolution transmission electron microscopy (HR-TEM, Jeol-JEM-2010) and a selected area diffraction pattern (SADP) analysis was operated at an accelerating voltage of 200 kV with a resolution of 0.19 nm. A differential thermal analysis was also conducted to study the thermal stability of the produced amorphous alloy using a Reometric STA 1500 differential thermal analyzer. The samples were placed in Al_2O_3 pans and heated in a dynamic argon atmosphere up to 1200 °C at different heating rates of 10, 20, and 30 °C/min.

3. RESULTS AND DISCUSSION

Figure 1 shows the XRD patterns of the Al-10%Fe-5%Ti-5%Ni powder mixture after different milling times. The XRD results demonstrate that in the early stages of milling, the intensity of the Fe, Ni, and Ti diffraction peaks decreases progressively. These changes suggest that these elements dissolve in the Al matrix and an Al solid solution forms during this early stage of the process. Another feature that can be seen in this pattern is a broadening of the Al diffraction peaks due to the reduction in the grain size, an increase in the lattice strain, and the formation of an amorphous phase. By increasing the milling time up to 40 h, only one halo ring remains in the XRD pattern. This point demonstrates that a fully amorphous phase is formed after this milling time. The TEM results of the sample presented in Fig. 2 are in agreement with the XRD findings. There is no significant change as the milling time prolonged to 100 h.

The differential thermal analysis (DTA) curves of the pro-

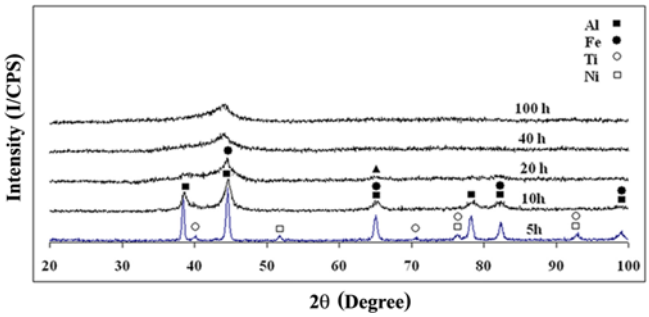

Fig. 1. XRD patterns of the Al-10%Fe-5%Ti-5%Ni powder mixture after various milling times.

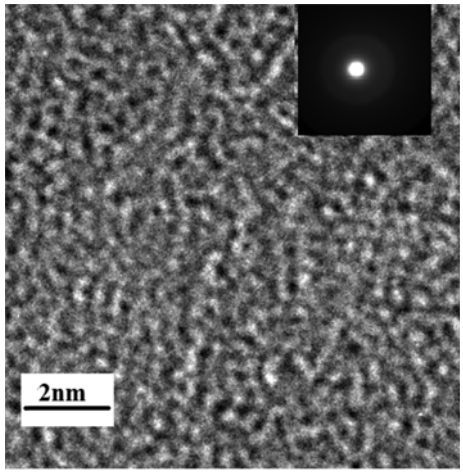

Fig. 2. TEM image of the Al-10%Fe-5%Ti-5%Ni powder mixture after 40 h of MA.

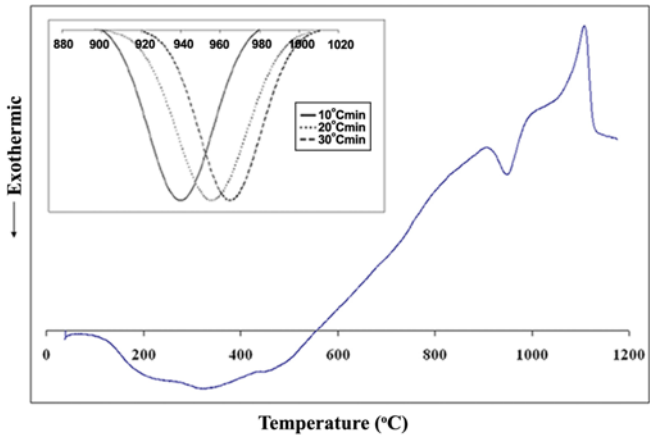

Fig. 3. DTA curves of the amorphous $Al_{80}Fe_{10}Ti_5Ni_5$ alloy at different heating rates.

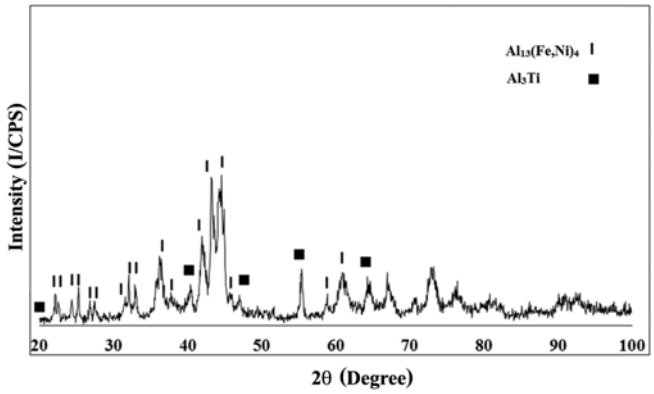

Fig. 4. XRD pattern of the amorphous $Al_{80}Fe_{10}Ti_5Ni_5$ alloy annealed at 1000 °C for 20 min.

duced amorphous phase after 40 h of milling at a constant heating rate of 20 °C/min is presented in Fig. 3. As seen, there is one exothermic (956 °C) and one endothermic (1110 °C) peak in this DTA curve. To analyze the reaction products responsible for the exothermic peak, the as-milled powder was annealed in an argon atmosphere at 1000 °C for 20 min. The XRD patterns of the annealed sample are presented in Fig. 4, where it can be seen that the XRD pattern for this sample consisted of nanocrystalline $Al_{13}(Fe,Ni)_4$ (40 nm) and Al_3Ti (10 nm) intermetallic peaks. Figure 5 shows that the high-resolution transmission electron microscope image of this sample is in agreement with the XRD result. As can be seen, two types of interplanar spacing d are recorded from the microstructure and correspond well with d(201)=0.2162 nm of $AlTi_3$ [27] and d(211)=0.39 nm of monoclinic $Al_{13}Fe_4$ [28]. Therefore, the exothermic peak in Fig. 3 can be attributed to the crystallization of the amorphous phase (amorphous $Al_{13}(Fe,Ni)_4$+Al_3Ti); hence, the crystallization mechanism is eutectic [7]. Meanwhile, the endothermic peak from Fig. 3 is related to the melting of the produced alloy.

According to the above results, the crystallization temper-

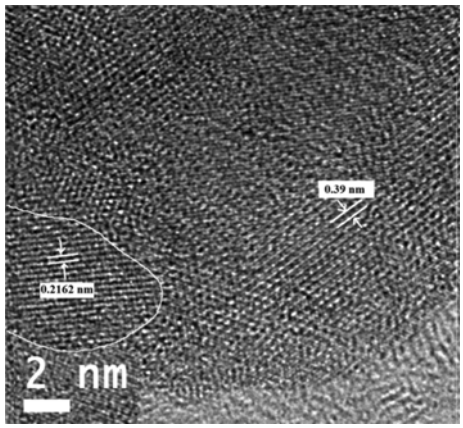

Fig. 5. HRTEM image of the amorphous $Al_{80}Fe_{10}Ti_5Ni_5$ alloy annealed at 1000 °C for 20 min.

ature of the amorphous $Al_{80}Fe_{10}Ti_5Ni_5$ alloy is approximately 956 °C. Although the crystallization temperature of this alloy is near the crystallization temperature of $Al_{80}Fe_{10}M_{10}$ (M=Ti, Ni, V) (in our previous study) amorphous alloys [12,14], it is much higher than the crystallization temperature of Al-Fe amorphous alloys such as $Al_{83}Fe_{17}$ and $Al_{85}Fe_{15}$ (below 650 °C) [29]. There are two explanations for this difference: i) The percentage of Al in the alloy: according to a previous study [7], by increasing the percentage of Al in Al-based amorphous alloys, the glass forming ability and the stability of the amorphous phase decrease. It is clear that the percentage of Al in $Al_{83}Fe_{17}$ and $Al_{85}Fe_{15}$ is higher than in the $Al_{80}Fe_{10}Ti_5Ni_5$ alloy. Obviously, $Al_{80}Fe_{10}Ti_5Ni_5$ has a higher thermal stability than the other Al-Fe amorphous alloys. ii) The presence of different alloying elements: According to the above results, the glass forming ability and thermal stability of the amorphous phase in Al-Fe alloys are low. By adding one or more alloying elements to these systems, the glass forming ability and thermal stability of the amorphous phase can be improved. In fact, the presence of Ni and Ti (good interaction elements with Al atoms) in $Al_{80}Fe_{10}Ti_5Ni_5$ is the main reason for the higher crystallization temperature of this alloy in comparison to other Al-Fe amorphous alloys [7,14].

The effective activation energy of the crystallization can be estimated using Kissinger's equation [30] as follows:

$$\ln\frac{\beta}{T_2} = \frac{E}{RT} + \text{const.} \quad (1)$$

where T is the highest temperature of the exothermic peak, β is the heating rate, R is the gas constant, and E is the effective activation energy of the crystallization. Kissinger's plot $\ln(\beta/T^2)$ versus $1/T$ results in approximately straight lines. Based on the slope of Kissinger's plots, the effective activation energy of the crystallization, estimated from the peak temperature of the exothermic peaks, is 538±5 kJ/mol, which is higher than the crystallization activation energy of

$Al_{80}Fe_{20}$ (200 kJ/mol) [13] and $Al_{80}Fe_{10}Ti_{10}$ (320 kJ/mol) [31] amorphous alloys. This point indicates that the thermal stability of the amorphous phase in the $Al_{80}Fe_{10}Ti_5Ni_5$ alloy (with the presence of Ni, Ti and Fe in the alloy) is more than $Al_{80}Fe_{20}$ (with the presence of Fe in the alloy) and $Al_{80}Fe_{10}Ti_{10}$ (with the presence of Ti and Fe in the alloy) alloys.

The area under the DTA curve is directly proportional to the total amount of crystallized alloy. The volume fraction α of the sample transformed into the crystalline phase during the crystallization event was obtained from the DTA curves (Fig. 3) as a function of the temperature, T, using the partial area method. It is important to note that before each study, the base line of DTA curves was removed using the NETZSCH software. The crystallized volume fraction α at any temperature T is given as $\alpha = (A_T/A)$, where A is the total area of the exothermic peak between the temperature T_i where the crystallization begins and the temperature T_f where the crystallization is completed, and A_T is the area between the initial temperature and any temperature T between T_i and T_f. The plots of α versus T at different heating rates are shown in Fig. 6. Their shapes are typical sigmoid shapes, which appear frequently in the literature [32-34]. The sigmoid plot exhibits bulk crystallization and excludes the chance of surface crystallization [34].

The local activation energy of the crystallization, which changes with the crystallization fraction, can be determined using the Flynn-Wall- Ozawa method [35,36]:

$$\log\beta = \log\frac{AE(x)}{g(x)R} - 2.315 - \frac{0.457E(x)}{RT}, \quad (2)$$

where A is the pre-exponential factor, $E(x)$ is the local activation energy of crystallization, and $g(x)$ is a function determined by the crystallization fraction. In fact, a plot of logβ versus $1000/T$ for the given values of the crystallization fraction gives the local activation energy of the crystallization. This method is employed to estimate the local activation energy of the crystallization of the $Al_{80}Fe_{10}Ti_5Ni_5$ amorphous alloy by analyzing the data in Fig. 6, and the results are shown in Fig. 7. It can be seen that the local activation energy increases slightly with the development of crystallization and then reaches a constant value when the crystallization fraction is more than 50%. This indicates that the crystallization process becomes more difficult as the temperature or crystallization fraction increases.

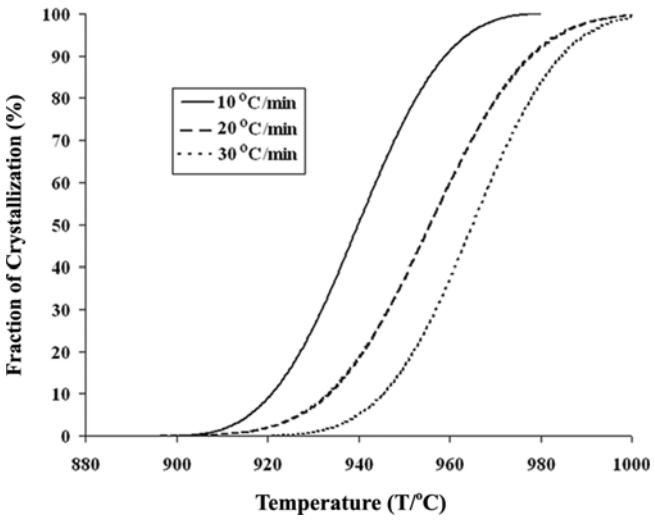

Fig. 6. Relationship between the crystallization fraction (x) and temperature (T) in the amorphous $Al_{80}Fe_{10}Ti_5Ni_5$ alloy.

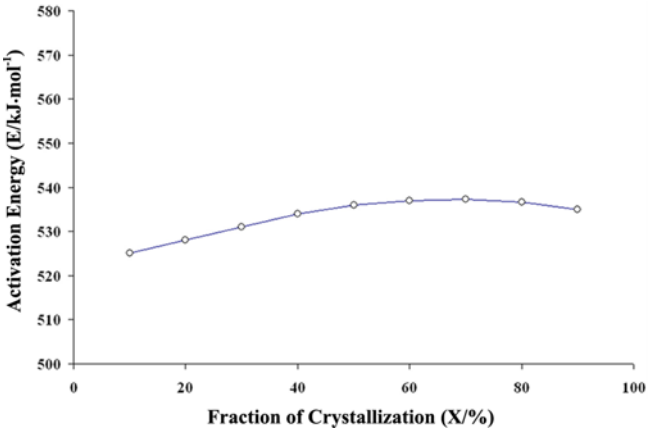

Fig. 7. Local activation energies of crystallization versus the crystallization fraction in the amorphous $Al_{80}Fe_{10}Ti_5Ni_5$ alloy.

The crystallization kinetics can be determined using the DTA and fitting the data with the Johnson-Mehl-Avrami (JMA) model as noted by Ozawa [37]:

$$\ln[-\ln(1-x)] = \ln\chi(T) - n\ln\beta, \quad (3)$$

where n is the Avrami exponent. The following formula was obtained after the transformation of Eq. (3) at a temperature T:

$$\left.\frac{d\{\ln[-\ln(1-x)]\}}{d\ln\beta}\right|_T = -n. \quad (4)$$

The Avrami exponent, n, were determined from the -ln[-ln(1-x)] versus lnβ plot. The results are presented in Fig. 8. It can be seen that the exponent, in the range of $1.5<n<2.5$, decreases as the temperature increases. The Avrami exponent provides detailed information of the nucleation and growth mechanisms. Ranganathan and Heimendahl [38] suggested that this exponent could be expressed as

$$n = a + bc, \quad (5)$$

where a is the nucleation index, which can range from 0 to 1 (a=0 for a nucleation rate of zero, $0<a<1$ for a nucleation rate decreasing with time, a=1 for a constant nucleation rate, and $a>1$ for an increasing nucleation rate), and b is the

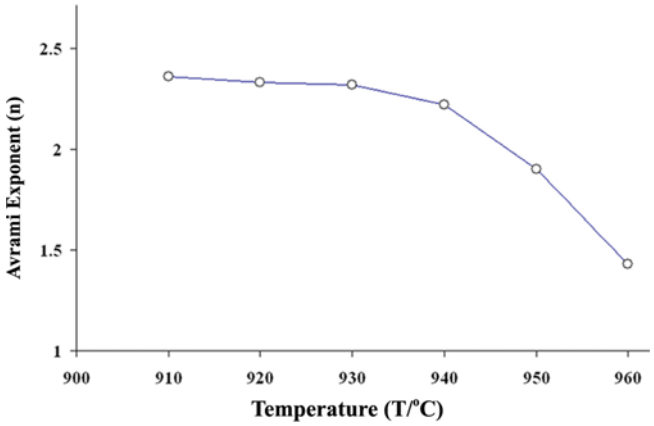

Fig. 8. Change of Avrami exponent with reference to the temperature.

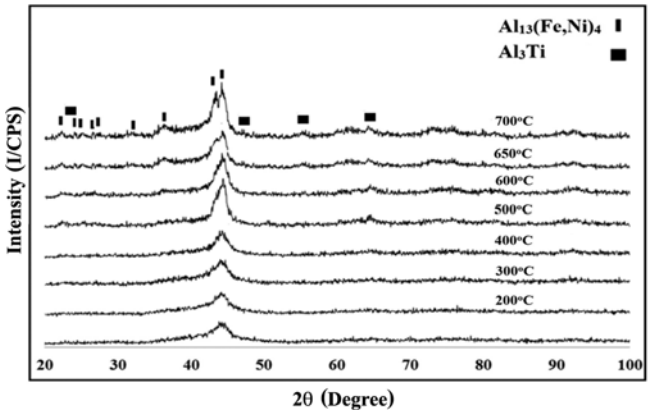

Fig. 9. XRD Patterns of $Al_{80}Fe_{10}Ti_5Ni_5$ amorphous phase after annealing at 200, 300, 400, 500, 600, 650, and 700 °C for 3 h.

dimension of the growth (with values 1, 2 or 3 for one, two, and three dimensional growth, respectively), and *c* is the growth index (*c*=1 for interface-controlled growth and *c*=0.5 for diffusion controlled growth). As for the $Al_{80}Fe_{10}Ti_5Ni_5$ amorphous alloy, the value of the index *a* was between 0 and 1, implying a 'decreasing nucleation rate,' that of the index *b* was equal to 3 corresponding to a 'sphere-type growth,' and the value of the growth index c was equal to 0.5 indicating a 'diffusion controlled growth.' This suggests that the crystallization of the $Al_{80}Fe_{10}Ti_5Ni_5$ amorphous alloy occurred with a decreasing nucleation rate and was governed by a three-dimensional diffusion-controlled growth.

The crystallization of amorphous phases is a diffusional process and is known to generally proceed by nucleation and growth processes. This process starts at temperatures in which diffusional processing starts and the diffusion rate increases with an increasing temperature. Crystallization studies of amorphous materials at lower temperature (under crystallization temperature) are interesting from many points of view. The results of such studies are helpful in understanding the mechanism and kinetics of phase transformation into the equilibrium state. They also allow us to evaluate the thermal stability of the amorphous state. Moreover, the crystallization studies make a controlled production of nano-structures possible [7].

In order to investigate the thermal stability and structural changes of the amorphous alloy at crystallization temperature, the as-milled powder particles (for 40 h) were annealed at several temperatures for 3 h. The XRD patterns of the as-milled and annealed samples at 200, 300, 400, 500, 600, 650, and 700 °C are presented in Fig. 9. Analysis of the XRD patterns, in Fig. 9, reveals that after annealing the powder mixture in temperatures below 400 °C, structural relaxation and stress relief processes was the only significant change that occurred in the amorphous phase, and no evidence of crystallization was found from the XRD patterns. In contrast, by annealing the samples above 400 °C (at crystallization temperature), nanocrystalline Al_3Ti and $Al_{13}(Fe,Ni)_4$ intermetallic phases precipitated from the amorphous matrix. As seen in Fig. 8, the intensity of these intermetallic peaks in the XRD patterns increased with an increasing annealing temperature. This indicated that the volume fraction of the nanocrystalline Al_3Ti and $Al_{13}(Fe,Ni)_4$ intermetallic phases that precipitated from the amorphous matrix increased at higher temperatures.

4. CONCLUSIONS

Based on our investigation of the crystallization kinetics of an $Al_{80}Fe_{10}Ti_5Ni_5$ amorphous alloy using a non-isothermal DTA analysis method, we summarize the primary results as follows. An amorphous $Al_{80}Fe_{10}Ti_5Ni_5$ alloy was obtained through mechanical alloying. The crystallization process of the $Al_{80}Fe_{10}Ti_5Ni_5$ amorphous alloy had one stage, which corresponded to the formation of the nanocrystalline $Al_{13}(Fe,Ni)_4$ (40 nm) and Al_3Ti (10 nm) intermetallic compounds. The crystallization activation energy for the produced amorphous phase evaluated through the Kissinger equation was 538±5 kJ/mol using the peak temperature of the exothermic reaction. The Avrami exponent or reaction order *n* was also discussed and indicated that the nucleation rate decreases with time and the crystallization is governed by a three-dimensional diffusion-controlled growth.

ACKNOWLEDGEMENTS

This work was supported by a National Research Foundation of Korea (NRF) grant funded by the Korea government (MEST) (No. 2010-0026981).

REFERENCES

1. J. H. Kim, J. S. Jo, W. J. Sim, and H. J. Im, *Korean J. Met. Mater.* **50**, 669 (2012).
2. H. K. Kim, J. H. Cho, H. W. Kim, and J. C. Lee, *Korean J. Met. Mater.* **50**, 503 (2012).

3. S. S. Shin, Y. H. Lim, E. S. Kim, and K. M. Lim, *Korean J. Met. Mater.* **50**, 531 (2012).
4. S. S. Kim, D. W Kim, and Y. S. Kim, *Korean J. Met. Mater.* **50**, 703 (2012).
5. H. S. Kim, *Mater. Sci. Eng. A* **251**, 100 (2001).
6. H. S. Seo, J. H. Gu, K. M. Park, J. S. Lee, J. H. Lee, and W. S. Chung, *Korean J. Met. Mater.* **50**, 897 (2012).
7. A. Inoue, *Prog. Mater. Sci.* **43**, 365 (1998).
8. C. Suryanarayana, *Prog. Mater. Sci*. **46**, 1 (2001).
9. H. S. Kim and S. I. Hong, *Acta Mater.* **47**, 2059 (1999).
10. H. S. Kim, *Mater. Sci. Eng. A* **304**, 327 (2001).
11. S. J. Hong, T. S. Kim, H. S. Kim, W. T. Kim, and B. S. Chun, *Mater. Sci. Eng. A* **271**, 469 (1999).
12. M. Tavoosi, M. H. Enayati, and F. Karimzadeh, *Met. Mater. Int.* **17**, 853 (2011).
13. F. Zhou, R. Luck, M. Scheffer, D. Lang, and K. Lu, *J. Non-Cryst. Solids* **250-252**, 704 (2011).
14. M. Tavoosi, F. Karimzadeh, M. H. Enayati, S.-H. Joo, and H. S. Kim, *J. Mater. Sci.* **467**, 633 (2011).
15. K. I. Kim and T. H. Hong, *Korean J. Met. Mater.* **49**, 264 (2011).
16. H. S. Kim, P. J. Warren, B. Cantor, and H. R. Lee, *Nanostruct. Mater.* **11**, 241 (1999).
17. H. Kato, K. Yubuta, D. V. Louzguine, A. Inoue, and H. S. Kim, *Scripta Mater.* **51**, 577 (2004).
18. D. N. Lee and H. S. Kim, *Powder Metall.* **35**, 275 (1992).
19. N. R. Park and I. J. Shon, *Korean J. Met. Mater.* **50**, 961 (2012).
20. I. J. Shon, H. Y. Song, S. W. Cho, W. B. Kim, and C. Y. Suh, *Korean J. Met. Mater.* **50**, 39 (2012).
21. S. L. Du, I. J. Shon, J. M. Doh, B. J. Park, and J. K. Yoon, *Korean J. Met. Mater.* **50**, 449 (2012).
22. S. H. Park, K. D. Woo, J. Y. Kim, and S. M. Kim, *Korean J. Met. Mater.* **50**, 469 (2012).
23. J. H. Jang and Y. H. Moon, *Korean J. Met. Mater.* **50**, 191 (2012).
24. W. B. Kim, H. J. Wang, K. M. Roh, S. W. Cho, J. W. Lim, and I. J. Shon, *Korean J. Met. Mater.* **50**, 310 (2012).
25. H. S. Kang, H. K. Park, J M. Doh, J. K. Yoon, B. J. Park, and I. J. Shon, *Korean J. Met. Mater.* **50**, 817 (2012).
26. G. K. Williamson and W. H. Hall, *Acta Metall.* **1**, 22 (1953).
27. JCPDS 50-0797.
28. JCPDS 14-0451.
29. M. Krasnowski and T. Kulik, *Mater. Chem. Phys*. **116**, 631 (1953).
30. H. E. Kissinger, *Anal. Chem*. **29**, 1702 (1957).
31. M. Tavoosi, M. H. Enayati, and F. Karimzadeh, *Powder Metall.* **54**, 445 (2011).
32. H. R. Wang, G. H. Min, Y. L. Gao, Y. F. Ye, and Y. F. Deng, *J. Alloys Compd.* **354**, 124 (2003).
33. C. Popescu, *Thermochim. Acta* **285**, 309 (1996).
34. A. Pratap, K. N. Lad, T. L. S. Rao, P. Majmudar, and N. S. Saxena, *J. Non-Cryst. Solids* **345-346**, 178 (2004).
35. J. H. Flynn, L. A. Wall, and A. Quick, *Polym. Lett*. **4**, 323 (1996).
36. T. Ozawa, *Bull. Chem. Soc. Jpn*. **38**, 1881 (1965).
37. T. Ozawa, *Polymers* **12**, 150 (1971).
38. S. Ranganathan and M. V. Heimendahl, *J. Mater. Sci.* **16**, 2401 (1981).